Raman Scattering and Nd^{3+} Laser Operation in NaLa(WO$_4$)$_2$

Alberto García-Cortés, Concepción Cascales, Alicia de Andrés, Carlos Zaldo, Evgenii V. Zharikov, Kirill A. Subbotin, Stefan Bjurshagen, Valdas Pasiskevicius, and Mauricio Rico

Abstract—The continuous-wave laser operation of Nd-doped tetragonal NaLa(WO$_4$)$_2$ crystal is studied at room temperature by optical pumping in the spectral region overlapping AlGaAs diode laser emission. This crystal has inhomogenously broadened optical bands. From the room-temperature spectroscopic parameters determined it is found that the optimum Nd concentration for the $^4F_{3/2} \rightarrow {}^4I_J$ laser channels must be in the 3–5 at.% range. For $J = 11/2$ and 13/2 channels ($\lambda \approx 1.06$ and 1.3 μm) the most favourable polarization configuration is parallel to the crystallographic c axis, while for $J = 9/2$ little polarization dependence of the laser efficiency is predicted. Laser operation was achieved with a 3.35 at.% Nd-doped sample grown by the Czochralski method. The laser operation was tested in an hemispherical optical cavity pumped by a Ti:sapphire laser. Stimulated emission at $\lambda = 1056$ nm was achieved for a wide spectral pumping range, $\lambda = 790$–820 nm. Stimulated Raman scattering was achieved in the picosecond regime with an efficiency similar to that of monoclinic KY(WO$_4$)$_2$ reference compound.

Index Terms—Disordered materials, laser tuning, NaLa(WO$_4$)$_2$, neodymium, Raman scattering, rare-earth optical spectroscopy, solid-state lasers.

I. INTRODUCTION

DOUBLE TUNGSTATES (DT) and double molybdates (DM) with general formula MT(XO$_4$)$_2$, M, T and X being monovalent, trivalent and W^{6+} or Mo^{6+} ions respectively, exhibit polymorphism (tetragonal, monoclinic and other crystalline phases) and may incorporate optically active lanthanides (Ln), up to the stoichiometric composition, i.e., complete substitution of T-ion of the host. For this reason they have attracted substantial attention as new materials for laser systems.

The laser operation studies of Nd^{3+}, Ho^{3+}, and Er^{3+} ions in DT started 40 years ago using flash lamps as excitation source [1]. It was soon realized that the distortions of the nearest environment of active ions in the monoclinic phase (α-phase) of KT(WO$_4$)$_2$ ($T = Y$ and Gd) grown at low temperatures in fluxes causes a marked anisotropy leading to very large peak optical cross sections in specific crystal orientations. Tetragonal scheelite-like DT and DM phases have Ln^{3+} integrated radiative transition probabilities very close to those of Ln^{3+}-doped α-KT(WO$_4$)$_2$ crystals, however, due to inhomogeneously broadened spectral bands, peak emission cross-sections in tetragonal DT and DM are substantially lower. For this reason the research on tetragonal DT and DM phases did not progress much despite they are the only phases that can be grown directly from their melts at much faster rates than those achievable for flux growth techniques. Nevertheless, some laser applications of tetragonal DT and DM have been performed. 1) Undoped hosts [NaBi(XO$_4$)$_2 X = W$, Mo, [2] and NaY(WO$_4$)$_2$, [3] have been proposed for laser line shifting by stimulated Raman scattering (SRS), and the SRS laser self-conversion was demonstrated in Nd-doped KLa(MoO$_4$)$_2$ [4] and NaLa(MoO$_4$)$_2$ [4], [5]. The advantage of tetragonal DT and DM over the monoclinic phases is their larger spontaneous Raman bandwidth [typically with full-width at half-maximum (FWHM)]FWHM ≈ 15 cm^{-1} for tetragonal and FWHM ≈ 5 cm^{-1} for the monoclinic phases), this allows for conversion of shorter laser pulses in the tetragonal phase, although with reduced Raman gain. Therefore, a tradeoff between these two properties must be obtained by searching for DT and DM hosts with intermediate FWHM. 2) The inhomogeneous broadening of the emission bands provides the opportunity to achieve tunable lasing in these media. Recently, under Ti:sapphire pumping, more than 40 nm of laser tunability around $\lambda = 1050$ nm has been shown in Yb^{3+} doped tetragonal DT an DM hosts, i.e., NaT(WO$_4$)$_2$ [6], $T = $ La, Gd, LiGd(MoO$_4$)$_2$ [6], and NaLa(MoO$_4$)$_2$ [6]. This wide tunability range allowed the production of 80 fs laser pulses in Yb-doped NaGd(WO$_4$)$_2$ by mode-locking [7]. 3) New laser technology requires pumping with semiconductor diode lasers. The inhomogeneous broadening of the absorption bands in tetragonal DT and DM is very favourable for laser diode pumping of the active medium, because thermal stabilization of pumping source is not critical in this case [8].

The physical basis of the large Raman and optical bandwidths in tetragonal DT and DM is the near to random occupancy of the same lattice sites by the M and T cations, creating a distribution of crystal fields on the optically active lanthanides [9]. From this perspective, the laser operation of lanthanides with the possibility of being excited by semiconductor diode lasers must be revised. Nd^{3+} is one of the obvious choices, since it can be pumped in the 800–810-nm region with AlGaAs diode lasers and several laser channels are possible using

$^4F_{3/2} \rightarrow {}^4I_{9/2}$ (890 nm), $^4F_{3/2} \rightarrow {}^4I_{11/2}$ (1.06 μm) and $^4F_{3/2} \rightarrow {}^4I_{13/2}$ (1.3 μm) emissions. Some previous information on spectroscopic properties and laser emission of Nd^{3+} in tetragonal DT and DM is already available, $NaT(WO_4)_2$, ($T =$ Bi [10]–[13]; Y [3], [14], [15]; La [16]–[18] and Gd [19], [20]), $NaT(MoO_4)_2$ ($T =$ Bi, [10]; Y, [21]; La, [17], [21]–[26], and Gd [21], [27]), $LiLa(WO_4)_2$, [28] $LiT(MoO_4)_2$ ($T =$ La, [17], [29], and Gd [17], [30]), $KLa(WO_4)_2$ [31]–[33], $KLa(MoO_4)_2$ [34], and $AgNd(WO_4)_2$ [35]. For $NaLa(WO_4)_2$ laser operation at 1063 [16] and 1335 nm [16] has been demonstrated only in pulsed regime and the spectroscopic features reported are nonpolarized. However, it is now well known that the laser active lanthanides, and in particular Nd^{3+}, exhibit strong dichroism in the above DT and DM tetragonal hosts.

In this work we show, for the first time to our knowledge, room-temperature 1.06 μm continuous-wave (CW) laser operation of Nd^{3+} in the $NaLa(WO_4)_2$ (hereafter NaLaW) single crystal host using a quasi-hemispherical linear cavity by pumping in the spectral region where efficient diode lasers are available. Moreover, we study the prospects for SRS applications and we discuss in a comparative manner the Nd spectroscopic properties in several DT and DM tetragonal crystals to determine the most suitable hosts for laser operation and tunability.

II. Crystal Growth and Host Characterization

Undoped and Nd-doped $NaLa(WO_4)_2$ (hereafter NaLaW) single crystals have been grown in air by the Czochralski method using Pt or Rh crucibles. Single-crystalline $CaWO_4$ bars cut parallel to the crystal c axis were used as seed. Two crystals with Nd molar substitution of 0.07 at.% and 3.5 at.% in the melt were grown. The preparation procedures are similar to those already described for other isostructural DT and DM hosts [5], [36]. Pulling and rotation rates were 3 mm/h and 10 r/min, respectively. The crystals were cooled down to room temperature at a rate of 100 $^\circ$C/h. To remove the thermo-mechanical stress the crystals were further annealed to 1000 $^\circ$C during 3 days and cooled to room temperature at 20 $^\circ$C/h. The neodymium concentration in the crystal was measured by proton induced X-ray emission spectroscopy in the sample with higher Nd doping in the melt (3.5 at.%). For this sample the Nd density in the crystal was $[Nd] = 2.0 \pm 0.4 \times 10^{20}$ cm^{-3} (3.35 at.%). Therefore, the Nd segregation coefficient in NaLaW is about 0.95. A neodymium density $[Nd] = 4 \times 10^{18}$ cm^{-3} (0.067 at.%) was calculated for the other Nd-doped crystal from the comparison of the optical absorption intensity with the sample above.

For optical measurements and laser demonstration, samples were oriented by Laue X-ray diffraction patterns and later the surfaces polished to scratch free grade. The sample orientation allowed the selection of $\sigma(\mathbf{E} \perp \mathbf{c})$ and $\pi(\mathbf{E} \parallel \mathbf{c})$ configurations for optical measurements, where $\mathbf{E}$ and $\mathbf{c}$ are the electric field of the light and optical axis of the crystal respectively.

Some preliminary measurements of the NaLaW refractive indexes (n) were limited to the 472–691-nm spectral range [37]. Using properly oriented prisms we have determined the refractive index in a wider spectral range 332–1525 nm. The crystal birefringence is found smaller than previously reported, namely $\Delta n < 0.005$. NaLaW exhibits an isotropic point, changing from
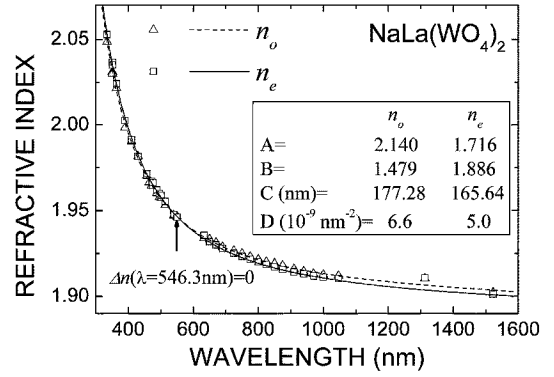

Fig. 1. Refractive indexes of NaLa(WO$_4$)$_2$ measured at 300 K (symbols) and the corresponding Sellmeier fits (curves).

slightly positive to negative uniaxial near 546 nm (Fig. 1). The dispersion of the refractive indexes has been fitted to single-pole Sellmeier equations containing an infrared correction term

$$n^2 = A + \frac{B}{1 - (C/\lambda)^2} - D\lambda^2 \tag{1}$$

The parameters $A, B, C,$ and D obtained from the fit are summarized in Fig. 1.

The spontaneous Raman scattering of NaLaW has been reported only at 300 K under unpolarized conditions [38]. We measured the polarized Raman spectra at 300 K in a backscattering geometry using configurations, $b(cc)\bar{b}$, $b(aa)\bar{b}$ and $b(ca)\bar{b}$, labelled according to the usual Porto notation. Raman spectra were obtained with a Jobin-Yvon HR 460 monochromator and a N_2 cooled CCD, exciting the samples with the 514.5-nm line of an Ar–Kr laser from Spectra-Physics. The incident and scattered beams were focused using an Olympus microscope and a Kaiser Supernotch filter was used to eliminate the elastically scattered light. The spectral Raman shift has been calibrated by using the 520-cm^{-1} phonon of a Si single crystal as reference. The most remarkable and new fact of the results now achieved for NaLaW is the presence of two well resolved Raman peaks 923 and 912 cm^{-1}, with FWHM of $\Delta\Omega_R = 7.5$ and 6.4 cm^{-1}, respectively. Another intense spontaneous Raman peak is found at 326.5 cm^{-1} but with larger FWHM, $\Delta\Omega_R = 12$ cm^{-1}. In other tetragonal DT and DM hosts, the two first Raman peaks are also found at similar phonon energy, but they appear unresolved inside an asymmetric single peak with large bandwidth, for instance 13 cm^{-1} in NaY(WO$_4$)$_2$, [3] and 14 cm^{-1} in NaGd(WO$_4$)$_2$ [39]. The calculated dephasing times, $T_R = [\pi c \Delta\Omega_R]^{-1}$, for the 923 and 912 cm^{-1} Raman peaks of NaLaW are $T_R = 1.4$ and 1.6 ps, respectively, and $T_R = 0.9$ ps for the 326.5 cm^{-1} peak. This suggests that NaLaW may efficiently support several steady state pumping regimes by using different phonon energies. In particular, by coupling to 923 and 912 cm^{-1} phonons the SRS properties are very similar to those achieved with the α-KT(WO$_4$)$_2$($T =$Gd, Y, Yb)[39] but using 326.5 cm^{-1} phonons a pulsed regime about two times shorter could be supported.

Considering the relatively large spontaneous Raman scattering linewidths in NaLaW we investigated further SRS by employing a near-infrared picosecond pump source. The pump source was a Ti:sapphire regenerative amplifier system
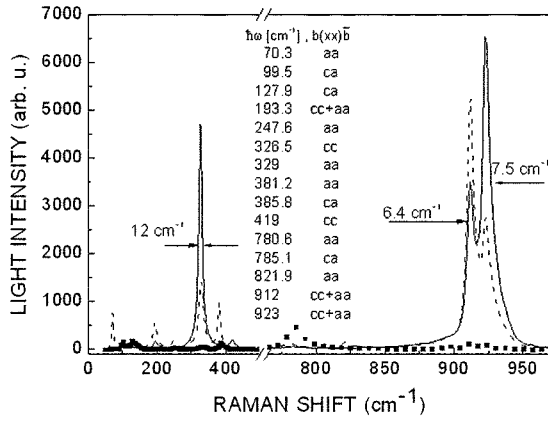
Fig. 2. The 300 K, spontaneous Raman scattering of tetragonal (a≡b) NaLa(WO$_4$)$_2$ single crystal. Continuous line: b(cc)$\bar{\text{b}}$ spectrum. Dashed line: b(aa)$\bar{\text{b}}$ spectrum. Points: b(ca)$\bar{\text{b}}$ spectrum.

operating in a picosecond pulse mode. The spectral width of the pump pulse was 14 cm^{-1} and the central wavelength was 822 nm. The pump pulse length could be varied between 1 and 70 ps without changing the spectral width by adjusting a compressor stage after the regenerative amplifier. The pump beam was focussed to a beam radius of 140 μm inside the 6.6-mm-long NaLaW sample. The sample was polished and left uncoated. For the crystal cut geometry we could separately investigate SRS for the b(cc)b and the b(aa)b configurations. For comparison of the SRS thresholds we used a 3-mm-long commercial α-KY(WO$_4$)$_2$ crystal where the beam was propagating along the crystal b axis, the typical configuration for Raman converters [40]. The output radiation after the crystal was collected by a 50-mm-diameter $f = 50$ mm lens and focused at the entrance slit of a spectrum analyzer (ANDO AQ-6315A). In order to prevent large pump intensities from saturating CCD array of the spectrum analyzer, a large part of the pump beam before the lens was blocked with small circular beam-block. Wide-angle collection optics was intentionally chosen in order to be able to measure SRS light possibly containing angular dispersion. This is especially important in the regime of transient SRS characterized by wide-angle SRS.

The SRS threshold in our case was determined by the pump intensity at which the measured signal-noise ratio of the first SRS line was 10 dB. The noise level was determined by the noise of the detection system and was -70 dBm which would correspond to the white-light spectral power density of about 0.1 nW/nm reaching the CCD array. Each spectral point is a result of integration over 20 laser pulses. This definition of the threshold is arbitrary because the SRS generation threshold has only a relative meaning in the devices without a cavity. So the SRS threshold in NaLaW was reached at the peak pump intensity in the focus of 4.6 GW/cm^2 for the pulse length of 1 ps. It should noted that this threshold intensity is comparable to that reported in NaBi(XO$_4$)$_2$ (X = Na or Mo) [2]. The measured SRS spectra for different pump intensities is shown in Fig. 3.

Fig. 3(a) shows the spectrum for the pump polarized parallel to the crystal c axis, i.e., b(cc)b configuration. There are several revealing features in the development of the spectrum. 1) Close to the SRS threshold the spectra are dominated by Stokes and anti-Stokes Ω_1 lines associated with 923 or 912
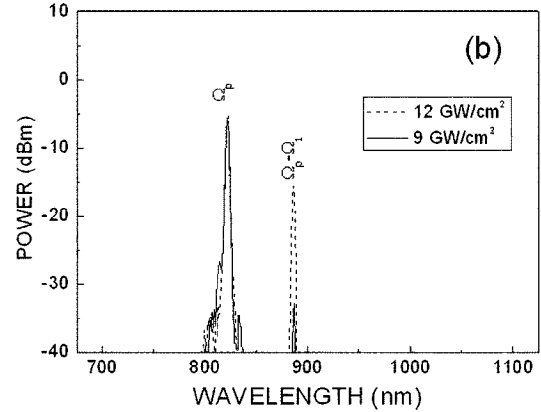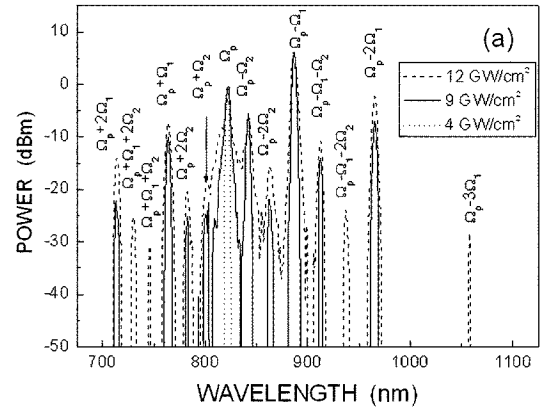

Fig. 3. SRS in NaLa(WO$_4$)$_2$ at different pump intensities and polarization configurations. (a) b(cc)b, dotted line: 4 GW/cm^2. Solid line: 9 GW/cm^2. Dashed line: 12 GW/cm^2. Ω_p is the pump frequency, phonon line. (b) b(aa)b, solid line: 9 GW/cm^2. Dashed line: 12 GW/cm^2.

cm^{-1} phonons. This is expected, considering that these phonons show the largest spontaneous Raman scattering efficiency. 2) The spectral lines are relatively narrow and have the width of about 25 cm^{-1} limited by the resolution of the spectral measurement. This indicates approximately stationary Raman response, thus confirming the large bandwidth acceptance inferred by the spontaneous Raman scattering spectrum in Fig. 2. 3) At pump intensity of 9 GW/cm^2 both Stokes and anti-Stokes cascades of Ω_1 line are generated along with cascades of new lines, Ω_2, associated with 326.5 cm^{-1} phonons. Moreover, it seems that Ω_1 and Ω_2 cascades start interacting, for instance $\Omega_p - \Omega_1 - \Omega_2$ Stokes line is generated by the $\Omega_p - \Omega_1$ Stokes. This is not surprising considering that Ω_1 is close to $3\Omega_3$ and in the presence of noticeable anharmonicity this interaction should be expected. 4) As the pump intensity is increased to 12 GW/cm^2 the anharmonicity-related spectral broadening and phonon-phonon interaction cascades become even more pronounced. At these pump intensities the SRS clearly acquires broad-band spectral and spatial scattering characteristics associated with the transient SRS regime. In contrast to the b(cc)b results presented up to now, the SRS threshold for b(aa)b configuration was approximately two-times higher and the spectrum contained only Ω_1 Stokes line as shown ion Fig. 3(b). The optical damage of the crystal surface limited the SRS spectra study with higher exciting intensities or with longer pulses.
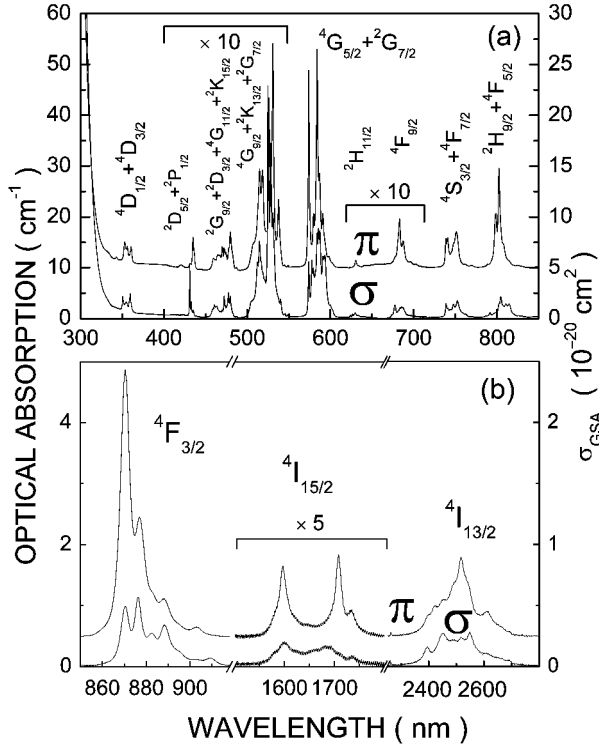
Fig. 4. Polarized optical absorption coefficient, α, of Nd^{3+} in $NaLa(WO_4)_2$ at room temperature. The ground state absorption cross section is calculated as $\alpha_{GSA} = \alpha/[Nd]$. The π spectrum has been vertically displaced for clarity.

In order to estimate Raman gain in NaLaW we measured SRS threshold in 3-mm-long α-$KY(WO_4)_2$. For 1-ps pulses, the threshold was about 11.5 GW/cm^2, while it decreased to 2.9 GW/cm^2 for 70-ps-long pulses. Considering that the spontaneous Raman linewidth of 905.6 cm^{-1} phonon mode in α-$KY(WO_4)_2$ is approximately the same as in NaLaW, [39] the SRS in both materials operate in similar regimes, i.e., close to transient SRS limit for 1-ps pump pulses. Taking into account different sample lengths and also uncertainties in determining threshold conditions we tentatively conclude that SRS in the 1-ps pump pulse regime gains in both materials are rather similar.

III. Nd^{3+} SPECTROSCOPIC CHARACTERIZATION

Fig. 4 shows the 300 K optical absorption of Nd^{3+} in NaLaW. Most of the bands are seen in both polarization configurations but with very different intensities see for instance the $^4F_{3/2}$ multiplet. Such dichroism is typical for Ln^{3+} doped tetragonal DT and DM crystals.

The NaLaW:Nd optical absorption spectra shown in Fig. 4 greatly improve the previous unpolarized spectroscopic results for this crystal [18]. In comparison to previous detailed studies on isostructural DT and DM hosts it also supposes a significant improvement. For instance, in comparison to NaBiW:Nd [12] the weak $^4I_{152} \rightarrow {}^2H_{11/2}$ and $\rightarrow {}^4F_{9/2}$ transitions are now determined and due to the larger ultraviolet transparency of the NaLaW host the $^4I_{15/2} \rightarrow {}^4D_{1/2} + {}^4D_{3/2}$ transitions close to 350 nm are observed. The presently calculated neodymium density in NaLaW has less uncertainty due to its high concentration with regards to previous studies with lower concentrated

TABLE I
300-K EXPERIMENTAL OSCILLATOR STRENGTHS $f_{exp}(\times 10^{-8})$ DETERMINED FROM THE OPTICAL ABSORPTION AND CALCULATED $f_{cal}(\times 10^{-8})$ USING THE Ω_K PARAMETERS. $\bar{\lambda}$ INDICATES THE MULTIPLET SPECTRAL BARYCENTER

$^4I_{9/2} \rightarrow {}^{2S+1}L_J$	$\bar{\lambda}$ [nm]	$f_{exp\sigma}$	$f_{exp\pi}$	$\overline{f_{exp}}$	f_{cal}
$^4I_{13/2}$	2508	87	147	107	122
$^4I_{15/2}$	1659	16	33	21	18
$^4F_{3/2}$	875	143	357	214	243
$^2H_{9/2} + {}^4F_{5/2}$	805	494	1205	731	687
$^4S_{3/2} + {}^4F_{7/2}$	749	474	925	625	637
$^4F_{9/2}$	684	37	74	49	54
$^2H_{11/2}$	631	14	9	12	15
$^4G_{5/2} + {}^2G_{7/2}$	586	4353	5556	4754	4761
$^4G_{9/2} + {}^2K_{13/2} + {}^4G_{7/2}$	526	839	984	887	791
$^2G_{9/2} + {}^2D_{3/2} + {}^4G_{11/2} + {}^2K_{15/2}$	473	144	236	175	133
$^2P_{1/2} + {}^2D_{5/2}$	433	44	79	56	72
$^4D_{1/2} + {}^4D_{3/2}$	356	934	1225	1031	1106

Ω_2 [cm^2]	Ω_4 [cm^2]	Ω_6 [cm^2]	RMS
11.36×10^{-20}	3.79×10^{-20}	3.27×10^{-20}	4.7×10^{-7}

Nd crystals. All these improvements of the experimental results add confidence to the following spectroscopic analyses.

In order to calculate the radiative properties of Nd^{3+} we use the Judd–Ofelt theory [41], [42]. Details on the application of this theory to the anisotropic DT and DM have been given in previous works [13], [43]. It should be mentioned here that the anisotropic optical absorption spectra have been averaged weighting by two the σ contribution. The refractive indexes were calculated at the average wavelength $\bar{\lambda}$ of each multiplet by interpolation of the results in Fig. 1. The largest uncertainty of this treatment arises from the error in the determination of the Nd density in the crystal. This leads to about 10% of uncertainty in the calculated radiative properties.

Table I provides the experimental oscillator strengths f_{exp} for each polarization and their average $\overline{f}_{exp}$ values. The Ω_k set obtained in Table I are close to those obtained for Nd^{3+} in $KLa(MoO_4)_2$, [33], with a $X = \Omega_4/\Omega_6 = 0.995$ parameter similar to that obtained for NaLaW, $X = 1.16$. The Ω_k set summarized in Table I has been used to calculate the radiative properties of Nd^{3+} in NaLaW. Table II summarizes some of the emission probabilities A, radiative branching ratios β, and radiative lifetime τ_{rad} for $^{2S+1}L_J$ multiplets up to $^4G_{9/2}$.

The radiative properties of the $^4F_{3/2}$ multiplet are of particular interest for lasing. The $^4F_{3/2}$ experimental lifetime of Nd^{3+} in DT and DM depends on concentration [13], [19], [21], [22], [32] and temperature [13]. To compare with the radiative lifetime calculated in Table II samples with low Nd concentration ($\leq 1 \times 10^{19}$ cm^{-3}) and measurements at low temperature (≤ 50 K) are necessary. Table III shows a literature compilation of the $^4F_{3/2}$ lifetimes reported for the tetragonal DT and DM hosts. We have made lifetime measurements for the two NaLaW:Nd (0.067 at.% and 3.35 at.% in the crystal) single crystals as well as for higher Nd concentrations using $NaLa_{1-x}$

TABLE II
Spontaneous Emission Probabilities A, Radiative Branching Ratios β, and Radiative Lifetime τ_{RAD} for $^{2S+1}L_J$ Multiplets of Nd^{3+} in NALA(WO$_4$)$_2$ Single Crystal. The Experimental Branching Ratios, β_{exp}, and Lifetimes, τ_{exp}, of the Lowest Concentrated Sample are Also Included for Comparison

Initial state	Final state	A [s^{-1}]	β_{th} [%]	β_{exp} [%]	τ_{rad} [μs]	τ_{exp}–T [μs]–[K]
$^4G_{9/2}$					13	
$^2G_{7/2}$					29	
$^4G_{7/2}$					19	
$^4G_{5/2}$					13.5	
$^4S_{3/2}$					0.2	
$^4F_{7/2}$					102	
$^4F_{5/2}$					145	
$^4F_{3/2}$	$^4I_{9/2}$	1679	47.1	52.3		209 - 5
	$^4I_{11/2}$	1629	44.4	42.9	276	176 -300
	$^4I_{13/2}$	302	8.1	4.8		
	$^4I_{15/2}$	16	0.4	----		
$^4I_{15/2}$					5223	
$^4I_{13/2}$					7350	
$^4I_{11/2}$					33203	

Nd$_x$(WO$_4$)$_2$ x =0.05, 0.1, 0.25, 0.5, 0.75 and 1 polycrystalline ceramics synthesized by solid-state reaction at 850 °C. Fig. 5 shows the results for the single crystal with lowest Nd concentration, $x = 0.00067$. A single exponential behavior was observed independently of excitation wavelength and temperature. The measured value was independent of the excited multiplet set, λ_{EXC} =514, 588, or 664 nm, see Fig. 5(a). The experimental lifetime increases only slightly with decreasing temperature, see Fig. 5(b). This thermal behavior is consistent with a multiphonon de-excitation processes

$$\tau_{ph}^{-1}(T) = \tau_{ph}^{-1}(0)(1+n)^{ph} \qquad (2)$$

where, $n = [\exp(\hbar\varpi/k_BT) - 1]^{-1}$, $\hbar\varpi \approx 917$ cm^{-1} is the energy of the phonon emitted and $ph = 6$ is the number of phonons required to maintain the energy conservation in a non-radiative transition between the $^4F_{3/2}$ and $^4I_{15/2}$ levels. A representative low temperature lifetime for low Nd-concentration ($x = 0.00067$) is 209 ± 7 μs. This lifetime is reduced to 176 μs at 300 K for the same Nd concentration and to 160 μs also at 300 K for the $x = 0.0335$ (3.35 at.%) Nd-doped NaLaW single crystal.

The light intensity decays observed for $x > 0.00067$ gradually show a departure from the single exponential law, see Fig. 6(a), and in parallel a marked decrease of total fluorescence output intensity is observed. For $0.00067 < x < 0.1$ the light intensity decays can be described by the model developed by Inokuti and Hirayama [44]. This model assumes energy transfer from an excited Nd^{3+} donor to the surrounding Nd^{3+} ions in the ground state continuously distributed. The light intensity decay follows the law

$$I(t) = I(0)\exp\left[\frac{-t}{\tau_0} - \Gamma\left(1 - \frac{3}{s}\right)\frac{N}{c_0}\left(\frac{t}{\tau_0}\right)^{3/s}\right] \qquad (3)$$

where $c_0 = 3/4\pi R_C^3$ is a critical concentration related to the distance R_C at which the donor-trap energy transfer rate equals the spontaneous decay rate, and $\Gamma(\times)$ is the gamma function evaluated in $\times$. The transfer mechanism can be deduced by plotting $\ln[I(t)/I(0)] + t/\tau_0$ versus $t^{3/s}$ and using the τ_0 value obtained for $x = 0.00067$ NaLaW:Nd. Fig. 6(a) shows the fits achieved for s = 6, i.e., dipole-dipole transfer. The fits provide the critical distance, R_C, for each concentration.

For $x \geq 0.25$ the weakness of the emission intensity allows to observe a first peak ($t < 10$ μs) corresponding to residual intensity of the excitation light, and a second one in the next 20 μs which most likely is related to the emission re-absorption. It must be noted that the 882 nm fluorescence emitted by the $^4F_{3/2}$ multiplet is efficiency absorbed, see Fig. 4(b). This fact contributes to an artificial delay in the emission. Despite this fact it is clear the $^4F_{3/2}$ emission intensity decay becomes faster with increasing Nd concentration as it can be qualitatively observed in Fig. 6(b).

For $x = 0.10$ the critical donor-acceptor distance $R_c = 0.58$ nm obtained is smaller than the average Nd-Nd distance $\bar{r} = (4\pi N/3)^{-1/3} = 0.74$ nm calculated assuming a uniform distribution of Nd ions. This clearly sets an upper limit for the Nd-dopant level useful for laser applications. However, the practical limit is even smaller since in these disordered DT and DM hosts Nd-Nd pairs occurs at low concentration of dopant due to the random occupancy of the T sites by Na, La, and Nd ions.

For practical diode pumping applications the $^2H_{9/2} + {}^4F_{5/2}$ multiplet set with absorption in the 795–815-nm range is used. Fig. 4 shows that the peak absorbance at 802 nm is significantly higher in π configuration, however, the broad spectral absorption range (FWHM is about 20 nm) easily covers the wavelength emission bandwidth of standard AlGaAs laser diodes around 810 nm, therefore, for excitation both polarization configurations are in principle of interest. Moreover, due to rather smooth shape of the absorption band the pumping efficiency of NaLaW:Nd should be almost insensitive to slight fluctuations of the diode emission wavelength, occurring due to instabilities of its temperature.

Fig. 7(a) and (b) shows a comparison of the fluorescence with the calculated emission cross section σ_{EMI} of the $^4F_{3/2} \rightarrow {}^4I_{9/2}$ channel. For this purpose we use the $^4F_{3/2}$ ground absorption cross section $\sigma_{GSA} = \alpha/[Nd]$ determined in Fig. 2 and the reciprocity method [45] which provides σ_{EMI} as

$$\sigma_{EMI} = \sigma_{GSA}\frac{Z_l}{Z_u}\exp\left(\frac{E_{z_l} - h\nu}{k_BT}\right) \qquad (4)$$

where the partition function ratio $Z_l/Z_u = 1.48$ and the low to up multiplet energy gap $E_{z_l} = 11418$ cm^{-1} have been used. The deviation observed in the π spectra at short wavelengths is attributed to fluorescence re-absorption.

For the $^4I_{11/2}$ and $^4I_{13/2}$ multiplets σ_{GSA} is not available, therefore, σ_{EMI} for the $^4F_{3/2} \rightarrow {}^4I_{11/2}$ and $^4F_{3/2} \rightarrow {}^4I_{13/2}$ channels must be calculated by the Füchtbauer–Ladenburg (F-L) method taken as reference the $\sigma_{EMI}({}^4F_{3/2} \rightarrow {}^4I_{9/2})$ previously determined. This can be made shortly as

$$\sigma_{EMI} = \sigma_{EMI}^{ref}\left({}^4F_{3/2} \rightarrow {}^4I_{9/2}\right)\frac{I}{I_{ref}}\frac{\lambda^5}{\lambda_{ref}^5}. \qquad (5)$$

Fig. 7(c)–(f) shows the results obtained.

TABLE III
SUMMARY OF REPORTED Nd^{3+} PROPERTIES AND THERMAL CONDUCTIVITY OF TETRAGONAL DT AND DM CRYSTAL HOSTS

|	τ_{rad} [μs]	τ_{exp} (T , [Nd]) [μs] ([K] , [at%])	$^4I_{9/2} \to {}^4F_{3/2}$ σ_{GSA} (λ) [10^{-20} cm^2] ([nm])		$^4F_{3/2} \to {}^4I_{11/2}$ σ_{EMI} (λ) [10^{-20} cm^2] ([nm])		Thermal cond. [mWcm^{-1}K^{-1}]		Ref
			σ	π	σ	π	(//a)	(//c)	
LiLaW	296	141 (300 , 4.3)	1.88 (805)		21.7 (1060)				28
NaYW			3 (804)	7.2 (801)	6 (1060)	1.2 (1336)	10.62	11.66	3,14
NaLaW	276	209 (5 , 0.7)	2.5 (804)	10.3 (802)	1.1 2.56 0.4	2.3 (870.6) 5.6 (1056) 1.1 (1336)			This work
NaGdW		180 (300 , 1)	3 (804)	16 (803)	5	9.4 (1058)	10.96	12.43	19, 20
NaBiW	142	143 (10 , 0.01)	7 (804)	38 (803)	9.9	16.3 (1058)			13
KLaW		210 (300 , 1.25)	5.8 (804)	22 (802)	2.1 (1060)				32
LiLaMo		160 (300 , 2)							29
LiGdMo		140 (300 , 3)			9-15 (1059.9)				30
NaYMo		140±10 (300 , <3)						23	21
NaLaMo		140±10 (300 , <3) 190 (300 , 1)						23	21,23 22
NaGdMo		140±10 (300 , <3) 94 (300 , 0.9)	3.7 (807)	15.9 (804)	1.9	1.7 (1060)		23	21,27
KLaMo	158	169 (10 , 5.27)	2.5	11.4 (808)	1.9 7.7 2.5	1.6 (892) 9.7 (1060) 3.2 (1336)			34
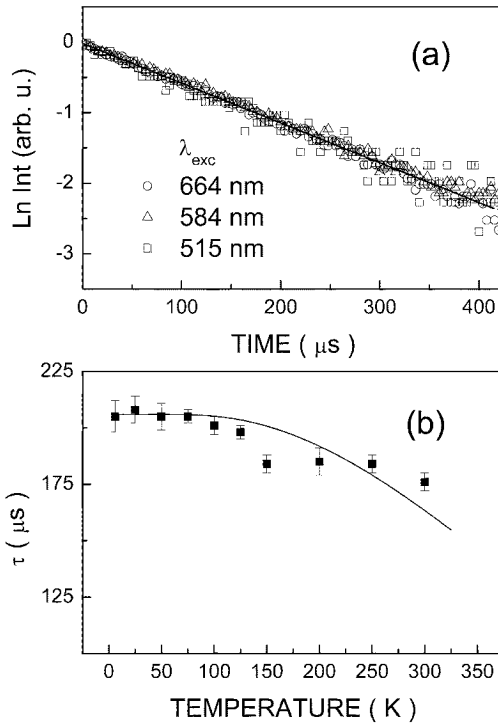
Fig. 5. Nd-doped NaLa(WO$_4$)$_2$ sample, [Nd] $= 4 \times 10^{18}$ cm^{-3}. (a) 300-K intensity decay of the photoluminescence Int at $\lambda_{EMI} = 882$ nm, excited at three different multiplet sets (see Fig. 4). (b) Temperature dependence of the $^4F_{3/2}$ lifetime τ, $\lambda_{EXC} = 664$ nm, $\lambda_{EMI} = 882$ nm. The points are the experimental results and the line is the fit obtained assuming $\overline{h}w = 923$ cm^{-1} for ph $= 5$ and $\overline{h}w = 385.8$ cm^{-1} for ph $= 1$ in (2). $\Delta E(^4F_{3/2} \to {}^4I_{15/2}) = 5360$ cm^{-1}.

Fig. 6. Dependence of $^4F_{3/2}$ lifetime with Nd concentration in NaLa$_{1-x}$Nd$_x$(WO$_4$)$_2$. $\lambda_{EXC} = 664$–669 nm, $\lambda_{EMI} = 882$ nm. (a) The points are the experimental results and the lines the fits: $x = 0.00067$ fit to single exponential, providing 176 μs. $x = 0.05$ and 0.10 fitted using the Inokuti–Hirayama model with $s = 6$. (b) Light-intensity decays for $x = 0.00067$ (points) given as reference and $x > 0.1$ (continuous lines).

As a first approximation the laser tunability range can be identified with the spectral range of σ_{EMI} for $^4F_{3/2} \to {}^4I_{11/2}$ and $^4F_{3/2} \to {}^4I_{13/2}$ emissions. For the $^4F_{3/2} \to {}^4I_{9/2}$ emission and due to the fluorescence re-absorption, the gain cross section $\sigma_{GAIN} = \beta\sigma_{EMI} - (1 - \beta)\sigma_{ABS}$ (β is the population in-

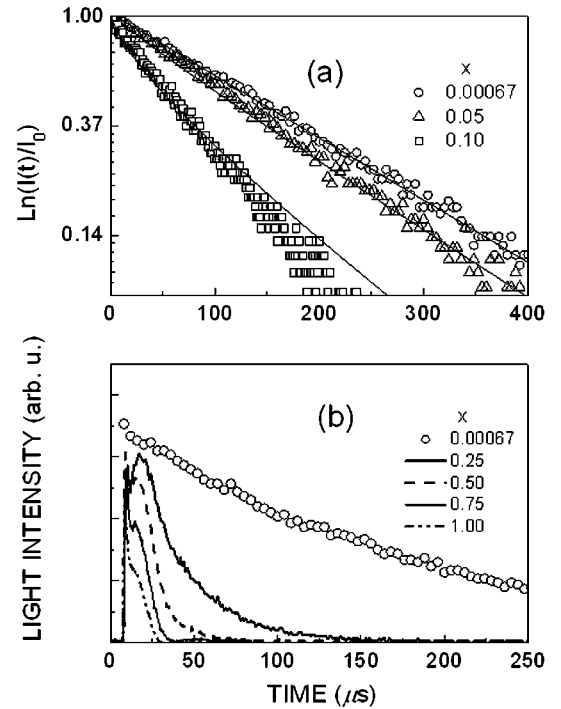version ratio) can be used as a reference of the laser tunability range. Fig. 8 shows the $^4F_{3/2} \to {}^4I_{9/2}$ σ_{GAIN} for $\beta = 0.2$–0.5. The gain cross section and the spectral ranges are rather similar for both polarizations. However, the larger cross sections of $\sigma_{EMI}(^4F_{3/2} \to {}^4I_{13/2})$ and $\sigma_{EMI}(^4F_{3/2} \to {}^4I_{11/2})$ in π-configuration suggest better laser efficiency and tunability ranges
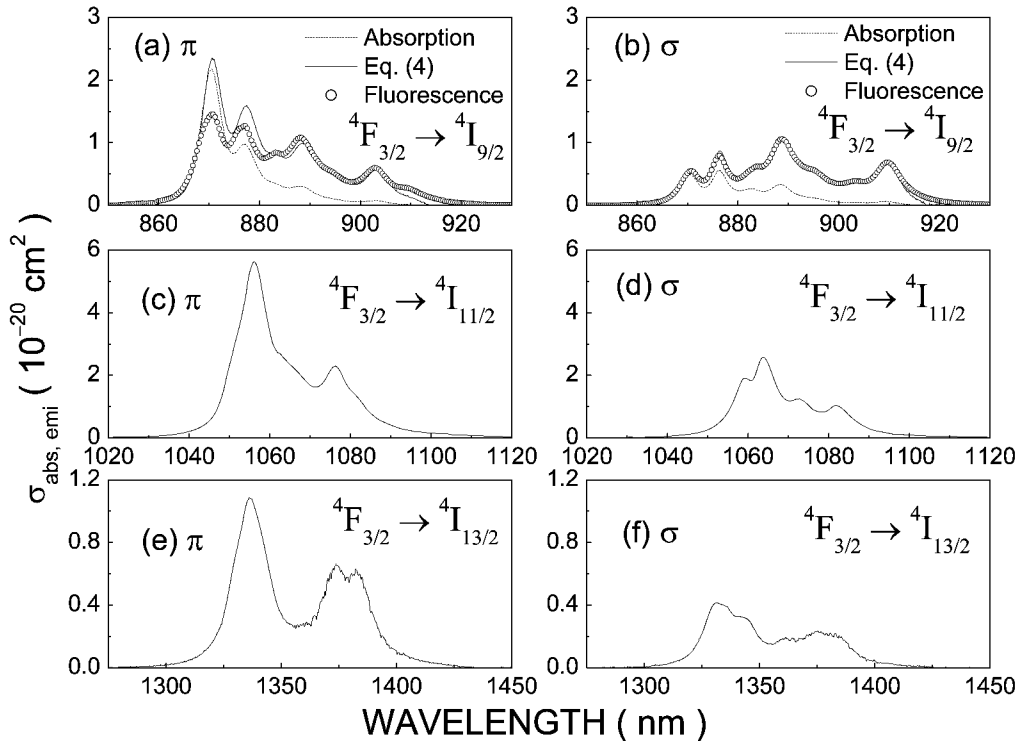
Fig. 7. 300-K polarized Nd^{3+} emission cross sections of $^4F_{3/2} \rightarrow {}^4I_J$ fluorescence channels in NaLa(WO$_4$)$_2$. (a)–(b) $J = 9/2$. The dashed line is the corresponding absorption cross section, the points are the experimental fluorescence and the solid lines are the emission cross sections calculated using (4). (c)–(d) $J = 11/2$. (e)–(f) $J = 13/2$. (c)–(f) Emissions cross sections calculated using (5).
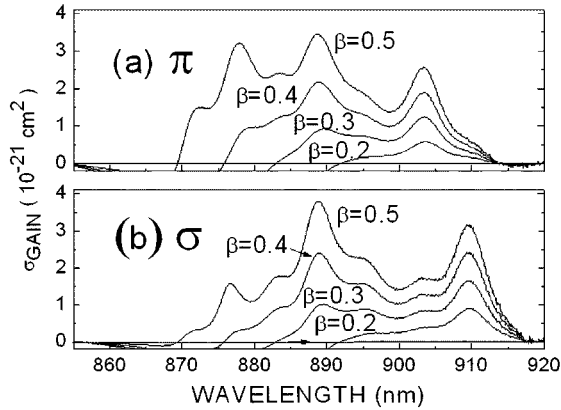

Fig. 8. Room-temperature $^4F_{3/2} \rightarrow {}^4I_{9/2}$ gain cross sections of Nd^{3+} in NaLa(WO$_4$)$_2$.

Fig. 9. Laser setup: L; Focal lens: $f = 150$ mm; mirror M1 radius of curvature $\mathrm{ROC} = -3000$ mm and mirror M$_2$ROC $= -100$ mm.

in this configuration. This is confirmed by the laser results presented in the next section.

IV. LASER EXPERIMENTS

For laser experiments we used an uncoated NaLaW:Nd ([Nd] $= 2 \times 10^{20}$ cm^{-3}) a-cut plate with a thickness of 6.515 mm along the pumping beam direction and passively cooled by a lateral face. The sample was set close to the input coupling mirror M$_1$ (HT at 800 nm and HR at 1060 nm) of a quasi-hemispherical linear cavity, see Fig. 9. The pump source was a Spectra Physics CW Ti:sapphire laser (model 3900) tuned in the spectral range of interest for laser diode pumping. The pump beam was focused inside the crystal by using a $f = 150$ m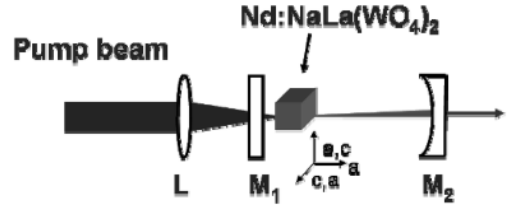m lens (L). The beam waist diameter of the pump was estimated to be about 45 μm. Two different output couplers, M$_2$, with 100 mm radius of curvature (ROC), were used, having high transmittance at 800 nm and two different transmission levels (T_{OC}) 0.2% and 3% at the used laser wavelength. The cavity length was optimized to 105 mm.

Laser radiation was achieved with π-polarized $(\mathbf{E}//\mathbf{c})$ pumping light. The emission was also spontaneously π-polarized, confirming the results of Fig. 7(c) and (d). Fig. 10 shows the input-output light intensity relationships. A lowest threshold of 104 mW and maximum output power of 168 mW were obtained with a $T_{\mathrm{OC}} = 3\%$. The slope efficiency was $\eta = 28\%$. No thermal degradation effects were observed under these conditions. The lasing emission wavelength λ_L shifts to shorter values with increasing T_{OC}, i.e., the lower intracavity power requires higher σ_{EMI}. In fact, $\lambda_L = 1056.4$ nm for $T_{\mathrm{OC}} = 3\%$ is just the wavelength corresponding to maximum σ_{EMI}, see Fig. 7(c).

The present laser efficiencies can be compared with some previous similar reports in other scheelite-like tetragonal DT and DM hosts. For instance: 1) about 183.8 mW of maximum laser output was obtained for a NaYW: 2%Nd sample, with 568 mW
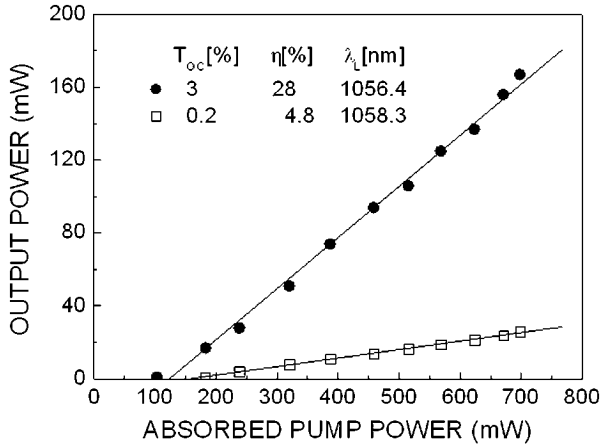
Fig. 10. Laser output power versus absorbed pump power (symbols) of Nd-doped NaLaW [Nd] $= 2 \times 10^{20}$ cm^{-3}, sample. The pump and emission were π-polarized ($\mathbf{E}//\mathbf{c}$). The linear fits (lines) give the slope efficiencies η for the two used T_{OC}.
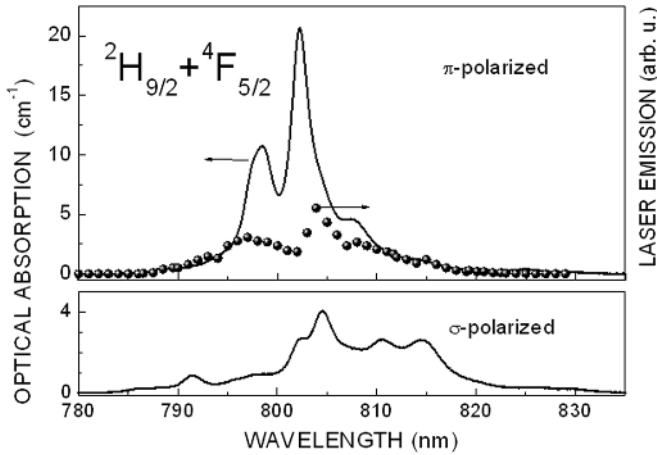

Fig. 11. Polarized ground state optical absorption cross sections (lines) of Nd^{3+} at the $^2H_{9/2} + {}^4F_{5/2}$ levels used for Ti:sapphire or diode pumping. π-polarized $\lambda \approx 1056$ nm laser output power versus pumping wavelength (points) for an incident pump power $P_{\text{inc}} = 740$ mW and $T_{OC} = 3\%$.

of CW Ti:sapphire absorbed power, i.e., $\eta = 38\%$ [14], [15]; 2) up to 130 mW of laser output was obtained in NaGdW:2%Nd with diode pumping and η up to 57% [20]; and 3) first laser experiments at NaLaMo:3.8%Nd crystal with diode pumping gave maximum output power about 100 mW with $\eta = 16.2\%$, [8] however, already slight optimization of laser cavity raise η up to 37% [46]. Direct comparison between these results is difficult due to the differences in experimental setups and antireflective coatings on the samples. Our present results (maximum output power and η) were limited by several facts; the most important ones are the presence of refractive index inhomogeneities developed during growth, a too large sample length and the lack of optimized T_{OC} or Nd-dopant level. After solving these limitations improved laser efficiency is expected.

The remarkable fact of NaLaW:Nd is the large bandwidth found for laser excitation. Fig. 11 shows a comparison of the σ and π GSA with the laser excitation spectral range. Clearly the laser excitation region includes all the absorption bandwidth. However, the laser output intensity is limited for large absorption values.

V. DISCUSSION

The most attractive feature of tetragonal DT and DM as Nd laser hosts is the possibility of emission wavelength control either by SRS coupling or by tuning inside the emission bandwidth and in the latter case eventually the application to obtain short laser pulses by mode-locking. Several host compositions can be used for this purpose. Table III shows some of the possible Li-, Na-, and K-based hosts in which Nd laser operation was demonstrated. In several previous works it was noted that above a certain Nd concentration the laser efficiency decreases due to concentration quenching of the photoluminescence. This effect is reflected in the reduction of the $^4F_{3/2}$ lifetime and of the overall emission intensity. The optimum Nd concentration in the crystal was reported to be 2 at.%–3 at.%. This conclusion is confirmed by the results here achieved for NaLaW:Nd. For Nd concentration above 5 at.% the samples show a strong reduction of the experimental fluorescence lifetime, however, the changes for $x < 0.05$ are small and suggest that the Nd concentration can be raised up to 5 at.% without degradation of the $^4F_{3/2}$ emission properties. Although 5 at.% is a relatively low dopant level for DT and DM of Y, La and Gd, in the case of Bi-based DT and DM these concentrations already cause some crystal defects. Therefore, $NaBi(XO_4)_2, X = W$ and Mo, and $LiBi(MoO_4)_2$ seem to be less suitable as Nd laser hosts.

The 300-K $^4F_{3/2}$ lifetimes of Nd-doped DM generally appear slightly smaller than in DT, see Table III. Therefore, better energy storage can be expected in DT, this behavior can not be ascribed to a higher multiphonon nonradiative de-excitation probability, since the cutting phonon energy of tetragonal DM are slightly smaller (<10 cm^{-1}) than those corresponding of isostructural DT. From this point of view Li-based tetragonal DT and DM could have some advantage since the maximum phonon energy slightly increases with the alkali ion atomic number, but the differences are again small, typically ≈ 890 cm^{-1} (Li), 915 cm^{-1} (Na) and 930 cm^{-1} (K). One possibility to explain the shorter lifetimes in DM would be a higher nonradiative probability related to excitation transfer to the host. This probability is represented by

$$W_{nr} = \tau^{-1}(0\,K) - \tau_{\text{rad}}^{-1} = \beta \exp(-\alpha \Delta E) \qquad (6)$$

also known as the *energy gap law*, where for a given lanthanide multiplet ΔE is the energy difference to the low lying energy level, and α and β characterize the host.

With the experimental information presently available for DT and DM is not possible to plot such law in different hosts. For a given host-ion-multiplet set, the lifetime $\tau(\text{T} = 0\ \text{K})$ must be determined in low concentrated samples in order to avoid concentration quenching, however, most of the lifetime values reported in literature correspond to high dopant levels (>1 at.%). Moreover, the obtained value must be compared to the calculated radiative lifetime which is scarcely available. In this work, we have determined suitable values for the $^4F_{3/2}$ transition of Nd^{3+} as well as for $^4S_{3/2}$ and $^4F_{9/2}$ of Er^{3+} in NaLaW. Fig. 12 shows a logarithmic representation of the *energy gap law* and Table IV summarizes the α and β parameters obtained from the fit in comparison to α-KGd(WO$_4$)$_2$ [47] and tetragonal Bi-based hosts [48]. Although this result for NaLaW is only an initial evaluation and other lanthanides should be
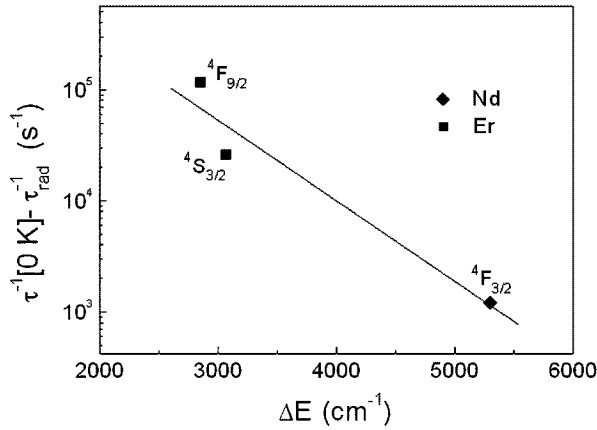
Fig. 12. Energy gap law representation for NaLa(WO$_4$)$_2$ crystal. ◆ $^4F_{3/2}$ transition of Nd^{3+}. ■ $^4S_{3/2}$ and $^4F_{9/2}$ of Er^{3+}.

TABLE IV
COMPARISON OF NONRADIATIVE PROPERTIES OF MONOCLINIC KGD(WO$_4$)$_2$
(α-KGW), AND TETRAGONAL, NABI(WO$_4$)$_2$, (NABIW), NABI(MOO$_4$)$_2$,
(NABIMO), LIBI(MOO$_4$)$_2$ (LIBIMO), AND NALA(WO$_4$)$_2$ CRYSTAL HOSTS

Hosts	β [s^{-1}]	α [cm]	Reference
α-KGW	1.4×10^7	1.4×10^{-3}	47
NaBiW-NaBiMo-LiBiMo	3.40×10^7	2.20×10^{-3}	48
NaLaW	0.79×10^7	1.67×10^{-3}	This work

considered in the future to include a wider range of ΔE, the results obtained are promising since they indicate comparatively low Nd^{3+} nonradiative losses by ion-host interactions in NaLaW.

Yb-doped DM have slightly higher absorption and emission cross-sections than Yb-doped DT [6], [49] but in this case laser efficiency is related to the gain cross section, σ_{GAIN}. For Nd this situation is also found for the $^4F_{3/2} \rightarrow {}^4I_{9/2}$ laser channel, but for the $^4F_{3/2} \rightarrow {}^4I_{11/2}$ and $^4F_{3/2} \rightarrow {}^4I_{13/2}$ channels the efficiency is proportional to the corresponding emission cross section. For Nd the differences between the reported σ_{GSA} of the hosts included in Table III are large, observe the factor 3 between NaYW with KLaW. However, the significance of these differences must be taken with reserve since there is yet not enough statistics. The large values reported for Nd doped NaBiW [13] are most likely overestimated due to experimental difficulties for determining accurate impurity concentration in low doped samples. The confidence on σ_{EMI} results for 1060 nm emission is even worse since they are calculated using lifetime results. More work is needed to determine the Nd^{3+} spectroscopic differences between these hosts. As a first approximation, it can be tentatively concluded that within the experimental uncertainties, the absorption $\left({}^4I_{9/2} \rightarrow {}^4F_{3/2}\right)$ and emission $\left({}^4F_{3/2} \rightarrow {}^4I_{11/2}\right)$ cross sections of Nd in scheelite-like tetragonal DT and DM are similar. In all hosts the absorption and emission cross sections of the laser related multiplets of Nd-ion are stronger for π-polarized light. A representative value for $\pi - \sigma_{GSA}$ at about 802 nm is $\approx 7–20 \times 10^{-20}$ cm^2 and for $\pi - \sigma_{EMI}$ at about 1060 nm is $\approx 6–10 \times 10^{-20}$ cm^2.

Once CW laser operation of Nd^{3+} in NaLaW has been demonstrated under pumping at the emission region of diode laser and

the optimum Nd concentration determined, further steps should be the demonstration of CW laser tunability and self-induced Raman shifting in the picosecond regime. Both applications seem rather feasible in NaLaW after implementing the required optical cavities. In particular the SRS efficiency of NaLaW is as large as in the standard α-KY(WO$_4$)$_2$ reference compound.

VI. CONCLUSION

First results of continuous Nd^{3+} laser emission in NaLaW at about 1056 nm have been achieved by pumping in the spectral region overlapping with AlGaAs diode laser emission. A broad excitation band of more than 20 nm can easily accommodate wavelength emission drifts of diode lasers. These first results show absence of thermal degradation of the laser active medium up to 700 mW of absorbed light power. The room-temperature Nd^{3+} spectroscopic properties in NaLaW have been characterized in detail. The results justify the better efficiency for laser operation of the π-configuration and determined the optimum Nd concentration for this purpose in the 3 at.%–5 at.% range. Stimulated Raman scattering efficiency of NaLaW were found larger also for π-configuration leading to a natural coupling between the emitted laser light without polarization selecting optical elements and the active Raman phonons. More systematic work is required to realize the actual Nd^{3+} spectroscopic differences between the tetragonal hosts studied up to now, but Nd^{3+} in DT appears with better storage energy capability than in isostructural DM crystalline hosts and in particular NaLaW host shows relatively low nonradiative losses by ion-host interaction.

REFERENCES

[1] A. A. Kaminskii, "Crystalline lasers: Physical processes and operating schemes," in *CRC Press Laser and Optical Science and Technology Series*, 1st ed. Boca Raton, FL: CRC Press, 1996.

[2] A. A. Kaminskii, S. N. Bagayev, K. Ueda, H. Nishioka, Y. Kubota, X. Chen, and A. Kholov, "Efficient stimulated Raman-scattering in tetragonal laser crystalline hosts NaBi(MoO$_4$)$_2$ and NaBi(WO$_4$)$_2$," *Jpn. J. App. Phys. 2*, vol. 34, pp. L1461–L1463, 1995.

[3] A. A. Kaminskii, H. J. Eichler, K. Ueda, N. V. Klassen, B. S. Redkin, L. E. Li, J. Findeisen, D. Jaque, J. García-Solé, J. Fernández, and R. Balda, "Properties of Nd^{3+}-doped and undoped tetragonal PbWO$_4$, NaY(WO$_4$)$_2$, CaWO$_4$, and undoped monoclinic ZnWO$_4$ and CdWO$_4$ as laser-active and stimulated Raman scattering-active crystals," *Appl. Opt.*, vol. 38, pp. 4533–4547, 1999.

[4] J. K. Viscakas and V. Syrusas, "Stimulated Raman scattering self-conversion of laser radiation and the potential for creating multifrequency solid-state lasers," *Soviets Phys. Coll.*, vol. 27, pp. 31–39, 1987, [Translated from Litovskii Fizicheskii Sbornik, vol. 27, pp. 547-558, 1987].

[5] A. V. Gulin, V. A. Pashkov, and N. S. Ustimenko, "SRS lasers with self-conversion of radiation frequency based on NaLa(MoO$_4$)$_2$:Nd^{3+} and KGd(WO$_4$)$_2$:Nd^{3+} crystals," in *Proc. SPIE, Laser Optics 2000: Solid-State Lasers*, 2001, vol. 4350, pp. 36–38.

[6] V. Petrov, M. Rico, J. Liu, U. Griebner, X. Mateos, J. M. Cano-Torres, V. Volkov, F. Esteban-Betegón, M. D. Serrano, X. Han, and C. Zaldo, "Continuous-wave laser operation of disordered double tungstate and molybdate crystals doped with ytterbium," *J. Non-Cryst. Solids*, vol. 352, pp. 2371–2375, 2006.

[7] S. Rivier, M. Rico, U. Griebner, V. Petrov, M. D. Serrano, F. Esteban-Betegón, C. Cascales, C. Zaldo, M. Zorn, and M. Weyers, "Sub-80 fs pulses from a mode-locked Yb:NaGd(WO$_4$)$_2$ laser," in *Proc. CLEO Eur.*, Jun. 2005, p. 359.

[8] E. V. Zharikov, D. A. Lis, A. M. Onishchenko, V. A. Romanyuk, K. A. Subbotin, S. N. Ushakov, and A. V. Shestakov, "Longitudially diode-pumped 1.06- μm Nd^{3+}:NaLa(MoO$_4$)$_2$ laser without pump- wavelength stabilization," *Quantum Electron.*, vol. 36, pp. 39–40, 2006.

[9] A. A. Kaminskii, "On the laws of crystal-field disorder of Ln^{3+} ions in insulating crystals," *Phys. Stat. Sol.*, vol. 102, pp. 389–397, 1987.

[10] A. A. Kaminskii, A. Kholov, P. V. Klevtsov, and S. Kh. Khafizov, "Spectroscopy and stimulated emission of Nd^{3+}-doped tetragonal $NaBi(MoO_4)_2$ and $NaBi(WO_4)_2$ disordered crystals," *Phys. Stat. Sol. A*, vol. 114, pp. 713–719, 1989.

[11] A. A. Kaminskii, A. Kholov, P. V. Klevtsov, and S. Kh. Khafizov, "Growth and generation properties of $NaBi(WO_4)_2$—Nd^{3+} single crystals," *Inorg. Mater.*, vol. 25, pp. 890–892, 1989, [Translated from Izv.Akad. Nauk SSSR, Neorg.Mater. vol. 25, pp. 1054-1056, 1989.

[12] A. Méndez-Blas, V. Volkov, C. Cascales, and C. Zaldo, "Growth and 10 K spectroscopy of Nd^{3+} in $NaBi(WO_4)_2$ single crystal," *J. Alloys Comp.*, vol. 323–324, pp. 315–320, 2001.

[13] A. Méndez-Blas, M. Rico, V. Volkov, C. Zaldo, and C. Cascales, "Optical emission properties of Nd^{3+} in $NaBi(WO_4)_2$ single crystal," *Molec. Phys.*, vol. 101, pp. 941–949, 2003.

[14] Z. Cheng, S. Zhang, K. Fu, J. Liu, and H. Chen, "Growth, thermal and laser properties of neodymium-doped sodium yttrium tungstate crystal," *Jpn. J. Appl. Phys.*, vol. 40, pp. 4038–4040, 2001.

[15] K. Fu, Z. Wang, Z. Cheng, J. Liu, R. Song, H. Chen, and Z. Shao, "Effect of Nd^{3+} concentration on the laser performance of a new laser crystal: $Nd:NaY(WO_4)_2$," *Opt. Laser Technol.*, vol. 33, pp. 593–595, 2001.

[16] N. D. Belousov, V. A. Kobzar-Zlenko, and B. S. Skorobogatov, "Spectra of a laser with a $CaWO_4:Nd^{3+}$–$LaNa(WO_4)_2:Nd^{3+}$ composite active medium," *Opt. Spectrosc.*, vol. 33, pp. 550–551, 1972, [Translated from Optika i Spektroskopiya, vol. 33, pp. 1002–1003, 1972.]

[17] A. A. Kaminskiii and S. E. Sarkisov, "Investigations of the stimulated emission due to $^4F_{3/2} \rightarrow {}^4I_{13/2}$ transition in Nd^{3+} ions in crystals," *Sov. J. Quant. Electron.*, vol. 3, pp. 248–249, 1973.

[18] N. S. Belokrinitskii, N. D. Belousov, V. I. Bonchkovskii, V. A. Kobzar-Zenklo, B. S. Skorobogatov, and M. S. Soskin, "Investigation of induced radiation of $LaNa(WO_4)_2$ single crystal activated with Nd^{3+}," *Ukrain. Fiz. Z.*, vol. 14, pp. 1400–1404, 1969.

[19] G. E. Peterson and P. M. Bridenbaugh, "Laser oscillation at 1.06 μm in the series $Na_{0.5}Gd_{0.5-x}Nd_xWO_4$," *Appl. Phys. Lett.*, vol. 4, pp. 173–175, 1964.

[20] N. Faure, C. Borel, M. Couchaud, G. Basset, R. Templier, and C. Wyon, "Optical properties and laser performance of neodymium doped scheelites $CaWO_4$ and $NaGd(WO_4)_2$," *Appl. Phys. B-Lasers*, vol. 63, pp. 593–598, 1996.

[21] A. A. Kaminskii, N. R. Agamalyan, L. P. Kozeeva, V. F. Nesterenko, and A. A. Pavlyuk, "New data on stimulated emission of Nd^{3+} ions in disordered crystals with scheelite structure.," *Phys. Stat. Sol. A*, vol. 75, pp. K1–K4, 1983.

[22] G. M. Zverev and G. Ya. Kolodnyi, "Stimulated emission spectroscopic investigations of double lanthanum-sodium molybdate with neodymium impurities," *Sov. Phys. JETP*, vol. 25, pp. 217–220, 1967, [Transl. Zhurnal Eksperimentalnoi i Teoreticheskoi Fiziki, vol. 52, pp. 337–341, 1967].

[23] A. M. Morozov, M. N. Tolstoi, P. P. Feofilov, and V. N. Shapovalov, "Luminescence and stimulated radiation of neodymium in lanthanum-sodium molybdate crystals," *Opt. Spectrosc.*, vol. 22, pp. 224–226, 1967.

[24] S. B. Stevens, C. A. Morrison, T. H. Allik, A. L. Rheingold, and B. S. Haggerty, "$NaLa(MoO_4)_2$ as a laser host material," *Phys. Rev. B*, vol. 43, pp. 7386–7394, 1991.

[25] A. V. Gulin, V. A. Pashkov, and N. S. Ustimenko, "SRS lasers with self-conversion of radiation frequency based on $NaLa(MoO_4)_2:Nd^{3+}$ and $KGd(WO_4)_2:Nd^{3+}$ crystals," in *Proc. SPIE Laser Optics 2000: Solid-State Lasers*, 2001, vol. 4350, pp. 36–38.

[26] A. A. Kaminskii, G. Ya. Kolodyni, and N. I. Sergeeva, "Continuous $LaNa(MoO_4)_2:Nd^{3+}$ laser operating at 300 K," *J. Appl. Spectrosc.*, vol. 9, pp. 1275–1276, 1968, [Translated from Zhurnal Prikladnoi Spektroskopii, vol. 9, pp. 884–886, 1968].

[27] X. Li, Z. Lin, L. Zhang, and G. Wang, "Growth, thermal and spectral properties of Nd^{3+}-doped $NaGd(MoO_4)_2$ crystal," *J. Cryst. Growth*, vol. 290, pp. 670–673, 2006.

[28] X. Y. Huang, Z. B. Lin, Z. S. Hu, L. Z. Zhang, J. S. Huang, and G. F. Wang, "Growth, structure and spectroscopic characterizations of Nd^{3+}-doped $LiLa(WO_4)_2$ crystal," *J. Cryst. Growth*, vol. 269, pp. 401–407, 2004.

[29] A. A. Kaminskii, A. A. Mayer, S. E. Sarkisov, and M. V. Provotor, "Investigation of stimulated emission from $LiLa(MoO_4)_2$-Nd^{3+} crystal laser," *Phys. Stat. Sol. A*, vol. 17, pp. K115–K117, 1973.

[30] A. A. Kaminskii, P. V. Klevtsov, K. S. Bagdasar, A. A. Maier, A. A. Pavlyuk, A. G. Petrosya, and M. V. Provotor, "New CW crystal lasers," *JETP Lett.*, vol. 16, pp. 387–389, 1972.

[31] X. Han and G. Wang, "Growth and spectral properties of $Nd^{3+}:KLa(WO_4)_2$ crystal," *J. Cryst. Growth*, vol. 249, pp. 167–171, 2003.

[32] X. Han and G. Wang, "Spectral characterizations of $Nd^{3+}:KLa(WO_4)_2$ crystal," *Mater. Res. Innov.*, vol. 7, pp. 65–67, 2003.

[33] X. Han, L. Zhang, M. Qiu, and G. Wang, "1.06 μm laser characteristics of $Nd^{3+}:KLa(WO_4)_2$ crystals," *Mater. Res. Innov.*, vol. 8, pp. 68–70, 2004.

[34] E. Cavalli, E. Zannoni, C. Mucchino, V. Carozzo, A. Toncelli, M. Tonelli, and M. Bettinelli, "Optical spectroscopy of Nd^{3+} in $KLa(MoO_4)_2$ crystals," *J. Opt. Soc. Amer. B*, vol. 16, pp. 1958–1964, 1999.

[35] C. Colón, A. Alonso-Medina, F. Fernández, R. Saéz-Puche, V. Volkov, C. Cascales, and C. Zaldo, "Correlation between polymorphism and optical bandwidths in $AgNd(WO_4)_2$," *Chem. Mater.*, vol. 17, pp. 6635–6643, 2005.

[36] Yu. K. Voron'ko, E. V. Zharikov, D. A. Lis, A. A. Sobol, K. A. Subbotin, S. N. Ushakov, V. E. Shukshin, and S. Dröge, "Growth and luminescent properties of $NaGd(WO_4)_2$: Yb^{3+} crystals," *Inorg. Mater.*, vol. 39, pp. 1509–1516, 2003.

[37] A. R. Gizhinskii, I. A. Bryzgalov, and I. A. Gribina, "Optical characteristics of single crystals of Na-La and Na-Y tungstates," *Inorg. Mater.*, vol. 8, pp. 1957–1958, 1972, [transl. from Izv. Akad. Nauk SSSR, Neorg. Mater., vol. 8, pp. 2219–2220, 1972].

[38] Yu. K. Voron'ko, A. A. Sobol, S. N. Ushakov, and L. I. Tsymbal, "Raman spectra and phase transformations of the $MLn(WO_4)_2$ (M = Na, K; Ln = La, Gd, Y, Yb) tungstates," *Inorg. Mater.*, vol. 36, pp. 947–953, 2000, [transl. from Izv. Akad. Nauk SSSR, Neorg. Mater., vol. 36, pp. 1130–1136, 2000].

[39] T. T. Basiev, A. A. Sobol, P. G. Zverev, V. V. Osiko, and R. C. Powell, "Comparative spontaneous Raman spectroscopy of crystals for Raman lasers," *Appl. Opt.*, vol. 38, pp. 594–598, 1999.

[40] A. S. Grabtchikov, A. N. Kuzmin, V. A. Lisinetskii, V. A. Orlovich, A. A. Demidovich, M. B. Danailov, H. J. Eichler, A. Bednarkiewicz, W. Strek, and A. N. Titov, "Laser operation and Raman self-frequency conversion in Yb:KYW microchip laser," *Appl. Phys. B*, vol. 75, pp. 795–797, 2002.

[41] B. R. Judd, "Optical absorption intensities of rare-earth ions," *Phys. Rev.*, vol. 127, pp. 750–761, 1962.

[42] G. S. Ofelt, "Intensities of crystal spectra of rare-earth ions," *J. Chem. Phys.*, vol. 37, pp. 511–520, 1962.

[43] A. Méndez-Blas, M. Rico, V. Volkov, C. Cascales, C. Zaldo, C. Coya, A. Kling, and L. C. Alves, "Optical spectroscopy of Pr^{3+} in $M^+Bi(XO_4)_2$, M^+ = Li or Na and $X = W$ or Mo, locally disordered single crystals," *J. Phys.: Condens. Mater.*, vol. 16, pp. 2139–2160, 2004.

[44] M. Inokuti and F. Hirayama, "Influence of energy transfer by exchange mechanism on donor luminescence," *J. Chem. Phys.*, vol. 43, pp. 1978–1989, 1965.

[45] D. E. McCumber, "Einstein relations connecting broad-band emission and absorption spectra," *Phys. Rev. A*, vol. 136, pp. A954–A957, 1964.

[46] E. V. Zharikov, Private Communication.

[47] M. C. Pujol, J. Massons, M. Aguiló, F. Díaz, M. Rico, and C. Zaldo, "Emission cross sections and spectroscopy of Ho^{3+} laser channels in $KGd(WO_4)_2$ single crystal," *IEEE J. Quantum Electron.*, vol. 38, no. 1, pp. 93–100, Jan. 2002.

[48] A. Méndez-Blas, "Espectroscopíaóptica de Lantánidos en Dobles Volframatos y Molibdatos Sin Transformación Polimórfica," Ph.D. dissertation, Univ. Autónoma Madrid, Madrid, Spain, 2003.

[49] Yu. K. Voron'ko, K. A. Subbotin, V. E. Shukshin, D. A. Lis, S. N. Ushakov, A. V. Popov, and E. V. Zharikov, "Growth and spectroscopic investigations of Yb^{3+}-doped $NaGd(MoO_4)_2$ and $NaLa(MoO_4)_2$—New promising laser crystals," *Opt. Mater.*, vol. 29, pp. 246–252, 2006.

Alberto García Cortés was born in Madrid, Spain, in 1980. He received the B.Sc. degree in physics from Autonomous University, Madrid, Spain, in 2003. Currently, he is working toward the Ph.D. degree in physics at the Institute of Materials Science of Madrid ICMM, Madrid, Spain, where he is researching crystal growth, crystallography, and optical properties of rare earths in double tungstates and molybdates.

Concepción Cascales received the Ph.D. degree in solid-state chemistry from the University Complutense of Madrid, Madrid, Spain, 1986.

After postdoctoral research at the CNRS, Meudon, France, she became a staff member of the Institute of Material Science of Madrid ICMM, Spanish Research Council CSIC. Currently, she is Senior Research Scientist. Her main research interests include the preparation of superconducting oxides, catalytic microporous compounds, and at present optical and laser materials, characterization crystallographic and magnetic structures, spectroscopic properties, and simulation of crystal field effects on rare-earth doped materials.

Alicia de Andrés received the Ph.D. degree in physics from Autonomous University of Madrid, Madrid, Spain, in 1987.

The regular use of synchrotron radiation facilities for materials characterization began after her postdoctoral research at LURE, France. Currently, she is Senior Research Scientist at the Material Science Institute of Madrid ICMM, Spanish Research Council CSIC, Madrid, Spain. Her main research interests are the characterization and optimization of materials properties with applications in spintronics and optoelectronics.

Carlos Zaldo was born in Madrid, Spain, in 1956. He received the Ph.D. degree in physics from Autonomous University, Madrid, Spain, in 1984.

In 1986, he joined the Institute of Materials Science in Madrid ICMM, a part of the Spanish Research Council, Madrid, Spain, where presently he is a Research Professor. His fields of research include preparation of laser crystals, pulsed laser deposition of thin films as well as structural, spectroscopic, and optical characterizations. Current projects deal with double tungstates and double molybdates laser applications and optical applications of ferroelectrics materials. He has co-authored about 140 papers and 90 conference communications.

Evgenii V. Zharikov was born in Moscow, Russia, in 1945. He received the Ph.D. from D.I. Mendeleyev Chemical Technology Institute, Moscow, Russia, in 1967, received the Ph.D. degree from P. N. Lebedev Physical Institute, USSR Academy of Sciences, in 1975 and the Professor degree from the General Physics Institute, USSR Academy of Sciences, in 1990.

Since 1995, he has been Head of the Department for Chemical Technology of Crystals, D. Mendeleyev University of Chemical Technology of Russia, Moscow. Also since 1987, he has been Head of the Laboratory of Laser Crystal Growth, A. M. Prokhorov General Physics Institute, Russian Academy Sciences, Moscow, Russia. His fields of research include growth and investigation of oxide laser crystals, carbon nanotubes, as well as influence of low-frequency vibrations onto crystal growth processes. He has co-authored about 250 papers and 200 Conference communications.

Kirill A. Subbotin was born in Vilnius, Lithuania, in 1970. He received the B.S. degree from the D.I. Mendeleyev University of Chemical Technology of Russia, Moscow, in 1993.

Since 1995, he has been working in the Laboratory of Laser Crystal Growth, A.M. Prokhorov General Physics Institute Russian Academy Sciences, Moscow, Russia. His fields of research include growth of oxide laser crystals by Czochralski and floating zone melting techniques, preparation of nanostructured glass-ceramics, and spectroscopic investigations of novel laser media. He has co-authored 30 papers and 41 Conference communications.

Stefan Bjurshagen was born in Södertälje, Sweden, in 1975. He received the Ph.D. degree in physics from the Royal Institute of Technology, Stockholm, Sweden, in 2005. His dissertation concerned diode-pumped rare-earth-doped quasi-three-level lasers.

His current work continues as a Researcher at the Royal Institute of Technology and includes optical spectroscopy and laser action of lanthanide-doped KRE(WO$_4$)$_2$ crystals.

Valdas Pasiskevicius received the Ph.D. degree from the Semiconductor Physics Institute, Vilnius, Lithuania, in 1996 where he carried out research in ultrafast optoelectronics, terahertz generation, and nonlinearities in semiconductors.

Since 1997, he has been with the Royal Institute of Technology, Stockholm, Sweden, where currently he is an Associate Professor. Main research interests include nonlinear optical materials, engineered nonlinear materials, nonlinear optical devices, novel laser materials, ultrafast optical parametric amplifiers, and terahertz generation. He is the author of about 90 articles and 130 conference contributions.

Dr. Pasiskevicius is a member of the Optical Society of America and the European Optical Society.

Mauricio Rico was born in Logroño, Spain, in 1973. He received the Ph.D. degree in physics from Autonomous University, Madrid, Spain, in 2003.

After postdoctoral research on solid-state laser based on Yb-doped materials (femtosecond pulses and continuous-wave laser operation) at Max-Born Institute for Nonlinear Optics and Short Pulse Spectroscopy, Berlin, Germany, he joined the Institute of Materials Science in Madrid ICMM, a part of the Spanish Research Council CSIC, Madrid, Spain, in 2006. His main research interests include spectroscopic and optical characterization of rare-earth ions in double tungstates or molybdates laser crystalline hosts, novel laser materials, ultrafast phenomena, and nonlinear optical materials and processes. He has co-authored more than 30 papers and 22 conference contributions.